# Second Thresholds in BEC-BCS-Laser Crossover of Exciton-Polariton Systems

Makoto Yamaguchi,[1,*] Kenji Kamide,[1] Ryota Nii,[1] Tetsuo Ogawa,[1,2] and Yoshihisa Yamamoto[3,4]

[1]*Department of Physics, Osaka University, 1-1 Machikaneyama, Toyonaka, Osaka 560-0043, Japan*
[2]*Photon Pioneers Center, Osaka University, 2-1 Yamada-oka, Suita, Osaka 565-0871, Japan*
[3]*National Institute of Informatics, 2-1-2 Hitotsubashi, Chiyoda-ku, Tokyo 101-8403, Japan*
[4]*E. L. Ginzton Laboratory, Stanford University, Stanford, California 94305, USA*

(Received 17 January 2013; published 12 July 2013)

The mechanism of second thresholds observed in several experiments is theoretically revealed by studying the BEC-BCS-laser crossover in exciton-polariton systems. We find that there are two different types of second thresholds: one is a crossover within quasiequilibrium phases and the other is into nonequilibrium (lasing). In both cases, the light-induced band renormalization causes gaps in the conduction and valence bands, which indicates the existence of bound electron-hole pairs in contrast to earlier expectations. We also show that these two types can be distinguished by the gain spectra.

DOI: 10.1103/PhysRevLett.111.026404 PACS numbers: 71.36.+c, 03.75.Gg, 71.35.Lk, 73.21.−b

In semiconductor exciton-polariton systems, Bose-Einstein condensation (BEC) of exciton-polaritons has been observed in recent years [1–6]. A hot issue is, now, how the exciton-polariton BEC, a thermal equilibrium phenomenon, changes into the lasing operation resulting from the electron-hole ($e$-$h$) plasma gain [7], which is essentially a nonequilibrium phenomenon [8,9]. Earlier experiments showed that there are two distinct thresholds when increasing the excitation density: the first one is the critical density for the BEC [10,11] and the second one is recognized as the standard lasing [10–15]. In most cases, the second-threshold mechanism is explained by a shift into the weak coupling regime due to dissociations of Coulomb-bound $e$-$h$ pairs (excitons) into the $e$-$h$ plasma. However, there is no convincing discussion why such dissociations lead to nonequilibration of the system essential for lasing. As another possibility, a new ordered state involving Bardeen-Cooper-Schrieffer (BCS)-like correlation is also speculated [16]. The second threshold is, thus, currently subject to intense debate. In this Letter, our purpose is to reveal the mechanism of the second threshold by studying the BEC-BCS-laser crossover theories [17–19]. As a result, we found that there are two different types of second thresholds: one is a crossover into photonic polariton BEC (quasiequilibrium) [20,21] and the other is into lasing (nonequilibrium) [22]. In both cases, the light-induced band renormalization causes gaps inside the conduction and valence bands, which indicates that there are still light-induced $e$-$h$ pairs even after the second thresholds, in contrast to the above scenario. We also show that these two types can be distinguished by the gain spectra.

Our model Hamiltonian is $\hat{H} = \hat{H}_S + \hat{H}_R + \hat{H}_{SR}$, where

$$\hat{H}_S = \hbar\sum_{\alpha,\boldsymbol{k}} \xi_{\alpha,\boldsymbol{k}} \hat{c}^\dagger_{\alpha,\boldsymbol{k}} \hat{c}_{\alpha,\boldsymbol{k}} + \hbar\sum_{\boldsymbol{q}} \xi_{\mathrm{ph},\boldsymbol{q}} \hat{a}^\dagger_{\boldsymbol{q}} \hat{a}_{\boldsymbol{q}} + \frac{1}{2}\sum_{\boldsymbol{k},\boldsymbol{k}',\boldsymbol{q}} \sum_{\alpha,\alpha'} U'_{\boldsymbol{q}} \hat{c}^\dagger_{\alpha,\boldsymbol{k}+\boldsymbol{q}} \hat{c}^\dagger_{\alpha',\boldsymbol{k}'-\boldsymbol{q}} \hat{c}_{\alpha',\boldsymbol{k}'} \hat{c}_{\alpha,\boldsymbol{k}} - \hbar\sum_{\boldsymbol{k},\boldsymbol{q}} (g^* \hat{a}_{\boldsymbol{q}} \hat{c}^\dagger_{c,\boldsymbol{k}+\boldsymbol{q}} \hat{c}_{v,\boldsymbol{k}} + \mathrm{H.c.}), \quad (1)$$

$$\hat{H}_R = \hbar\sum_{\alpha,\boldsymbol{k}} \xi^B_{\alpha,\boldsymbol{k}} \hat{b}^\dagger_{\alpha,\boldsymbol{k}} \hat{b}_{\alpha,\boldsymbol{k}} + \hbar\sum_{\boldsymbol{p}} \xi^B_{\boldsymbol{p}} \hat{\Psi}^\dagger_{\boldsymbol{p}} \hat{\Psi}_{\boldsymbol{p}}, \quad (2)$$

$$\hat{H}_{SR} = \hbar\sum_{\alpha,\boldsymbol{k},\boldsymbol{q}} \Gamma^\alpha_{\boldsymbol{k}} \hat{c}^\dagger_{\alpha,\boldsymbol{k}} \hat{b}_{\alpha,\boldsymbol{q}} + \hbar\sum_{\boldsymbol{p},\boldsymbol{q}} \zeta_{\boldsymbol{q}} \hat{a}^\dagger_{\boldsymbol{q}} \hat{\Psi}_{\boldsymbol{p}} + \mathrm{H.c.}, \quad (3)$$

are the system, reservoir, and their interaction Hamiltonians, respectively, where $\alpha, \alpha' \in \{c, v\}$ [19]. In Eq. (1), $\hat{c}_{c,\boldsymbol{k}}$ ($\hat{c}_{v,\boldsymbol{k}}$) is the conduction (valence) band electron annihilation operators with the electronic dispersion $\xi_{c/v,\boldsymbol{k}} \equiv \omega_{c/v,\boldsymbol{k}} \mp \hbar^{-1}\mu/2$, $\hat{a}_{\boldsymbol{q}}$ is the cavity photon annihilation operator with the photonic dispersion $\xi_{\mathrm{ph},\boldsymbol{q}} \equiv \omega_{\mathrm{ph},\boldsymbol{q}} - \hbar^{-1}\mu$, and $\hbar^{-1}\mu$ is an oscillation frequency of the photon and polarization fields, which corresponds to the energy of the main peak in photoluminescence. The carriers are interacting with each other through the Coulomb interaction $U'_{\boldsymbol{q}}$, and they can emit photons via the light-matter coupling constant $g$. Similarly, in Eqs. (2) and (3), $\hat{b}_{c,\boldsymbol{k}}$ and $\hat{b}_{v,\boldsymbol{k}}$ denote fermion annihilation operators of pumping baths and $\hat{\Psi}_{\boldsymbol{p}}$ is a boson annihilation operator of free-space vacuum fields. In this model, Eqs. (2) and (3) are responsible for the incoherent fermionic pumping and photon decay (see the Supplemental Material [23]). Based on the above Hamiltonians, we focus on steady states described by the polarization function $p_{\boldsymbol{k}} \equiv \langle \hat{c}^\dagger_{v,\boldsymbol{k}} \hat{c}_{c,\boldsymbol{k}} \rangle$, the number of electrons $n_{e,\boldsymbol{k}} \equiv \langle \hat{c}^\dagger_{c,\boldsymbol{k}} \hat{c}_{c,\boldsymbol{k}} \rangle$ and holes $n_{h,-\boldsymbol{k}} \equiv 1 - \langle \hat{c}^\dagger_{v,\boldsymbol{k}} \hat{c}_{v,\boldsymbol{k}} \rangle$, and a coherent photon field formed in the

 

$\boldsymbol{q} = 0$ state $\langle \hat{a}_{\boldsymbol{q}} \rangle = \delta_{\boldsymbol{q},0} a_0$ with the oscillation frequency $\hbar^{-1}\mu$. These are the minimum variables for describing the BEC, BCS states, and semiconductor lasers.

The band renormalization of the $e$-$h$ system can, then, be conveniently studied by the poles of the single-particle spectral function $A_{\alpha\alpha}(\nu;\boldsymbol{k})$. Within the Hartree-Fock approximation (HFA), a standard Green's function technique yields

$$A_{cc/vv}(\nu;\boldsymbol{k}) = 2|u_{\boldsymbol{k}}|^2 L(\nu, \mp E_{\boldsymbol{k}}) + 2|v_{\boldsymbol{k}}|^2 L(\nu, \pm E_{\boldsymbol{k}}), \quad (4)$$

where $\sqrt{2}u_{\boldsymbol{k}} \equiv [1 + \tilde{\xi}^{+}_{eh,\boldsymbol{k}}/E_{\boldsymbol{k}}]^{1/2}$ and $\sqrt{2}v_{\boldsymbol{k}} \equiv e^{i\theta_{\boldsymbol{k}}}[1 - \tilde{\xi}^{+}_{eh,\boldsymbol{k}}/E_{\boldsymbol{k}}]^{1/2}$ with $E_{\boldsymbol{k}} \equiv [(\tilde{\xi}^{+}_{eh,\boldsymbol{k}})^2 + |\Delta_{\boldsymbol{k}}|^2]^{1/2}$ are the Bogoliubov coefficients, $L(\nu, \pm E_{\boldsymbol{k}}) \equiv \hbar\gamma/[(\hbar\nu - \hbar\tilde{\xi}^{-}_{eh,\boldsymbol{k}} \pm \hbar E_{\boldsymbol{k}})^2 + (\hbar\gamma)^2]$ is the Lorentz function, $\Delta_{\boldsymbol{k}} = |\Delta_{\boldsymbol{k}}| e^{i\theta_{\boldsymbol{k}}} \equiv g^* a_0 + \hbar^{-1}\sum_{\boldsymbol{k}'} U'_{\boldsymbol{k}'-\boldsymbol{k}} p_{\boldsymbol{k}'}$ is a composite order parameter, and $\gamma$ is the thermalization rate of the $e$-$h$ system (see the Supplemental Material [23]). In the derivation, the notation is transformed into the $e$-$h$ picture with $\tilde{\xi}^{\pm}_{eh,\boldsymbol{k}} \equiv (\tilde{\xi}_{e,\boldsymbol{k}} \pm \tilde{\xi}_{h,\boldsymbol{k}})/2$, where $\tilde{\xi}_{e/h,\boldsymbol{k}} \equiv \omega_{e/h,\boldsymbol{k}} + \Sigma^{\mathrm{BGR}}_{e/h,\boldsymbol{k}} - \hbar^{-1}\mu/2$ describes the single particle energy renormalized by the Coulomb interactions $\hbar\Sigma^{\mathrm{BGR}}_{e/h,\boldsymbol{k}} \equiv -\sum_{\boldsymbol{k}'} U'_{\boldsymbol{k}'-\boldsymbol{k}} n_{e/h,\boldsymbol{k}'}$, including the band-gap renormalization (BGR).

In Eq. (4), there are remarkable similarities to superconductivities [24]. It is then clear that $\min[2\hbar E_{\boldsymbol{k}}]$ represents the gap energy opened at $\mu/2$ in the renormalized conduction and valence bands [typically Figs. 1(a) and 1(b)]. Such a picture is well known, for e.g., the BEC-BCS crossover but, now, one should notice that Eq. (4) is also applicable for *lasing* [22] because thermal equilibrium is not required

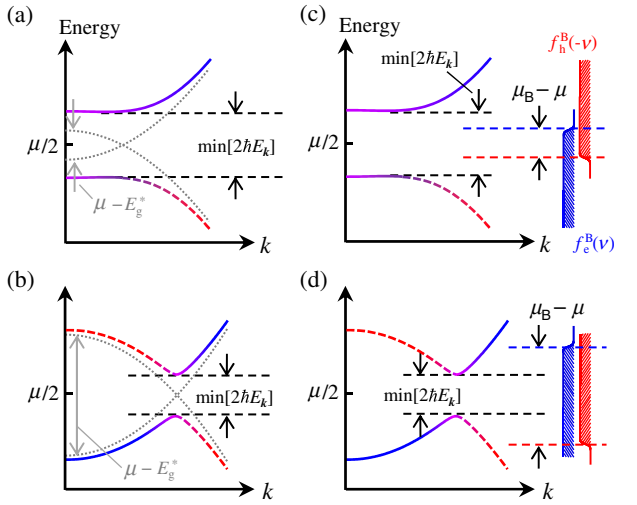


FIG. 1 (color online). Renormalized conduction bands for (a) large ($|\mu - E^*_g| \lesssim \min[2\hbar E_{\boldsymbol{k}}]$) and (b) small ($\min[2\hbar E_{\boldsymbol{k}}] \lesssim \mu - E^*_g$) gap energies. Here, $E^*_g \equiv E_g + \hbar\Sigma^{\mathrm{BGR}}_{e,\boldsymbol{k}=0} + \hbar\Sigma^{\mathrm{BGR}}_{h,\boldsymbol{k}=0}$ and the gray dotted lines show the energies by ignoring $\Delta_{\boldsymbol{k}}$ in $E_{\boldsymbol{k}}$. Relations to $f^B_{e/h}(\pm\nu)$ are also illustrated in panel (c) for quasiequilibrium [condition (I)] and panel (d) for lasing [condition (II)]. $\omega_{e,k} = \omega_{h,k}$ and $\mu^B_e = \mu^B_h$ are assumed.

in the derivation. In this case, $\mu$ is not the chemical potential but the laser frequency. Furthermore, the gap is opened at $\mu/2$ whenever lasing because $a_0 \neq 0$ and $p_{\boldsymbol{k}} \neq 0$ result in $\min[2\hbar E_{\boldsymbol{k}}] \neq 0$. The origin of the gap is analogous to the Rabi splitting in resonance fluorescence [25–28]. This can be understood from the expression of $\min[2\hbar E_{\boldsymbol{k}}] = 2\hbar|g|\sqrt{n_{\mathrm{ph}}}$ ($n_{\mathrm{ph}} \equiv |a_0|^2$) obtained by assuming free electrons ($U'_{\boldsymbol{q}} = 0$) with $\mu > E_{\mathrm{g}}$ ($E_{\mathrm{g}}$; the bare band gap energy), which is equivalent to the Rabi frequency in resonance fluorescence. Hence, it is worth noting that the existence of the gap indicates that light-induced $e$-$h$ pairs do exist whenever lasing even though there is no $e$-$h$ pair before lasing. This is one of our important results despite the quite simple analysis.

For later convenience, two typical situations for large and small gap energies are shown in Figs. 1(a) and 1(b), respectively. In Fig. 1(a), the renormalized conduction band has a gap around $k \approx 0$ with flattened dispersions because $e$-$h$ band mixing occurs for large $k$ regions. In contrast, in Fig. 1(b), the renormalization is mainly focused on particular $k$ regions. In both cases, the renormalized bands have gaps at $\mu/2$ and the same holds for the valence band (not shown).

In order to discuss the second-threshold mechanism, however, the unknown variables $a_0$, $p_{\boldsymbol{k}}$, $n_{e,\boldsymbol{k}}$, $n_{h,\boldsymbol{k}}$, and $\mu$ in Eq. (4) should be determined in a comprehensive way including BEC, BCS, and laser physics [17–19]. Within the HFA, the simultaneous steady-state equations, derived from Eqs. (1)–(3), can formally be written as

$$\partial_t a_0 = 0 = -i\tilde{\xi}_{\mathrm{ph},0} a_0 + ig\sum_{\boldsymbol{k}} p_{\boldsymbol{k}} - \kappa a_0, \quad (5)$$

$$\partial_t p_{\boldsymbol{k}} = 0 = -2i\tilde{\xi}^{+}_{eh,\boldsymbol{k}} p_{\boldsymbol{k}} - i\Delta_{\boldsymbol{k}} N_{\boldsymbol{k}} - 2\gamma(p_{\boldsymbol{k}} - p^0_{\boldsymbol{k}}), \quad (6)$$

$$\partial_t n_{e/h,\boldsymbol{k}} = 0 = -2\Im[\Delta_{\boldsymbol{k}} p^*_{\boldsymbol{k}}] - 2\gamma(n_{e/h,\boldsymbol{k}} - n^0_{e/h,\boldsymbol{k}}), \quad (7)$$

where $N_{\boldsymbol{k}} \equiv n_{e,\boldsymbol{k}} + n_{h,\boldsymbol{k}} - 1$ is the population inversion and $\kappa$ is the photon loss rate. Note that Eqs. (5)–(7) have well-known forms of the Maxwell-semiconductor Bloch equations (MSBEs) under the relaxation time approximation (RTA) if $n^0_{e/h,\boldsymbol{k}}$ is replaced by the Fermi distribution with $p^0_{\boldsymbol{k}} = 0$ [7,19,27,29]. In general, the MSBE under the RTA can describe the physics of semiconductor lasers but cannot describe the BEC and BCS states. However, the key point here is that Eqs. (5)–(7) become able to describe the BEC, BCS, and laser physics in a unified way when $p^0_{\boldsymbol{k}}$ and $n^0_{e/h,\boldsymbol{k}}$ are described by

$$p^0_{\boldsymbol{k}} \equiv i\int \frac{d[\hbar\nu]}{2\pi}\{G^R_{cv,\boldsymbol{k}}(\nu)[1 - f^B_h(-\nu)] - G^{R*}_{vc,\boldsymbol{k}}(\nu) f^B_e(\nu)\},$$

$$n^0_{e/h,\boldsymbol{k}} \equiv \int \frac{d[\hbar\nu]}{2\pi} f^B_{e/h}(\nu) A_{cc/vv}(\pm\nu;\boldsymbol{k}),$$

where $f^B_{e/h}(\nu) \equiv [\exp\{\beta[\hbar\nu - (\mu^B_{e/h} - \mu/2)]\} + 1]^{-1}$ is the bath Fermi distribution with the chemical potential

$\mu^B_{e/h}$. The exact expression of $G^R_{\alpha\alpha',\boldsymbol{k}}$ is given in the Supplemental Material [23]. Then, by assuming $\omega_{e,\boldsymbol{k}} = \omega_{h,\boldsymbol{k}}$ and a charge neutrality $\mu^B_e = \mu^B_h$ with $\mu_B \equiv \mu^B_e + \mu^B_h$, it can be shown that Eqs. (5)–(7) can recover the BCS gap equation when (I) $\min[2\hbar E_{\boldsymbol{k}}] \gtrsim \mu_B - \mu + 2\hbar\gamma + 2k_BT$ (quasiequilibrium). In contrast, there appear $k$ regions described by the MSBE when (II) $\mu_B - \mu \gtrsim \min[2\hbar E_{\boldsymbol{k}}] + 2\hbar\gamma + 2k_BT$ (lasing; nonequilibrium). The physical meanings of these conditions are discussed in detail in Ref. [19] (see also the Supplemental Material [23]) and not repeated here. Instead, these conditions are illustrated in Figs. 1(c) and 1(d) in relation to $f^B_{e/h}(\pm\nu)$ for quasiequilibrium and lasing conditions, respectively. It is, then, clear that the system enters into lasing phases when $\mu_B - \mu$ roughly goes beyond the energy gap $\min[2\hbar E_{\boldsymbol{k}}]$ by ignoring the broadening due to $\gamma$ and $T$.

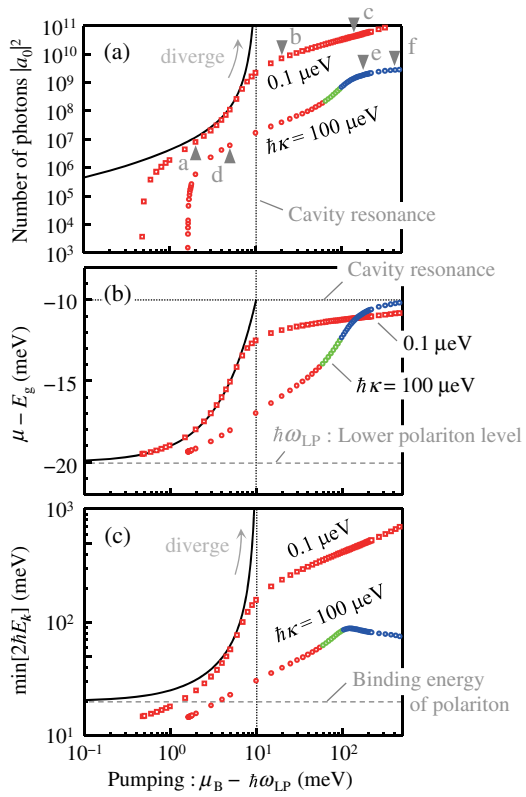


FIG. 2 (color online). Numerical solutions of (a) the number of photons $|a_0|^2$, (b) the oscillation frequency $\mu$, and (c) the gap energy $\min[2\hbar E_{\boldsymbol{k}}]$ as a function $\mu_B$ for $\hbar\kappa = 0.1$ $\mu$eV (squares) and 100 $\mu$eV (circles). Red and blue colors are used when satisfying the quasiequilibrium condition (I) and the lasing condition (II) in the text, respectively. Green colors are used when both of them are not satisfied. As a result, plots for $\hbar\kappa = 100$ $\mu$eV can be divided into three regimes: quasiequilibrium (red, $\mu_B - \hbar\omega_{LP} \lesssim 6.0 \times 10^1$ meV), crossover (green, $6.0 \times 10^1$ meV $\lesssim \mu_B - \hbar\omega_{LP} \lesssim 1.0 \times 10^2$ meV), and lasing (blue, $1.0 \times 10^2$ meV $\lesssim \mu_B - \hbar\omega_{LP}$). In contrast, all plots for $\hbar\kappa = 0.1$ $\mu$eV are in quasiequilibrium regime (red). For comparison, black solid lines show the results by thermal-equilibrium theories [20,21].

Based on the above formalism, we have performed numerical calculations, where the cavity level ($= \hbar\omega_{ph,0}$) is in resonance with the (1S) exciton level located at 10 meV below $E_g$ and the lower polariton level $\hbar\omega_{LP}$ is formed at 20 meV below $E_g$ (see the Supplemental Material [23]). For $\hbar\kappa$, we have used values of 0.1 $\mu$eV and 100 $\mu$eV to study the effects of nonequilibrium. We note, however, that $\hbar\kappa = 100$ $\mu$eV is a reasonable value in current experiments. Figure 2 shows the calculated results of $|a_0|^2$, $\mu$, and $\min[2\hbar E_{\boldsymbol{k}}]$ as a function of $\mu_B$, the pumping parameter. In the case of the equilibrium theories, $|a_0|^2$ diverges in the limit of $\mu_B \to \hbar\omega_{ph,0}$ because it is preferable to increase photons rather than electrons and holes due to the phase space filling effects. As a result, the photonic polariton BEC is achieved by the photon-mediated $e$-$h$ attraction [20,21]. In contrast, in the case with finite pumping and losses (plots), the behaviors are different in many aspects. Focusing on the plots for $\hbar\kappa = 0.1$ $\mu$eV, two distinct thresholds can be seen ($\mu_B - \hbar\omega_{LP} \approx 5.0 \times 10^{-1}$ meV and $6.0 \times 10^0$ meV) in Fig. 2(a). At the same time, $\mu$ is gradually blueshifted from $\hbar\omega_{LP}$ and then approaches the bare cavity resonance [Fig. 2(b)]. Similar qualitative behaviors also can be seen for $\hbar\kappa = 100$ $\mu$eV. These behaviors are consistent with experiments. However, there is a crucial difference between the two; according to the above-mentioned conditions (I) and (II), all plots are in quasiequilibrium for $\hbar\kappa = 0.1$ $\mu$eV but there are plots (blue, $\mu_B - \hbar\omega_{LP} \gtrsim 1.0 \times 10^2$ meV) in lasing for $\hbar\kappa = 100$ $\mu$eV after the second threshold.

The difference is also reflected in $n_{e,k}$ and $p_k$, as shown in Fig. 3. Before the second thresholds, $n_{e,k}$ and $p_k$ for $\hbar\kappa = 0.1$ $\mu$eV [Fig. 3(a)] are similar to those for $\hbar\kappa = 100$ $\mu$eV [Fig. 3(d)]. However, after the second thresholds, $n_{e,k}$ and $p_k$ are quite different, depending on the value

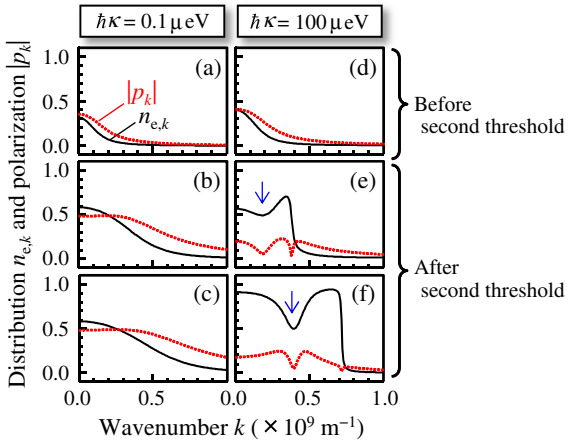


FIG. 3 (color online). Calculated distributions $n_{e,k}$ and polarizations $|p_k|$ corresponding to the triangles indicated by a–f in Fig. 2(a). Panels (a)–(c) are for $\hbar\kappa = 0.1$ $\mu$eV and panels (d)–(f) are for $\hbar\kappa = 100$ $\mu$eV. Arrows show the kinetic hole burning.

of $\hbar\kappa$. In the case of $\hbar\kappa = 0.1$ $\mu$eV, $n_{e,k}$ monotonically decreases as a function of $k$ and $p_k$ has a plateau $\approx 0.5$ [Figs. 3(b) and 3(c)], which are the same features as the photonic polariton BEC in quasiequilibrium [20,21]. In contrast, in the case of $\hbar\kappa = 100$ $\mu$eV, the kinetic hole burning appears as a signature of lasing and the Fermi surface is formed with the population inversion $n_{e,k} > 0.5$ [Fig. 3(e)]. For larger $\mu_B$, such behaviors become much more pronounced [Fig. 3(f)]. These results directly show that the second thresholds for $\hbar\kappa = 0.1$ $\mu$eV and 100 $\mu$eV in Fig. 2(a) are formed by different mechanisms.

In fact, for $\hbar\kappa = 0.1$ $\mu$eV, the second threshold is formed by the same mechanism as the photon divergence in the equilibrium theories, and therefore, it results from the crossover into the photonic polariton BEC. In the present case, there are finite losses of cavity photons even if the system is in quasiequilibrium. As a result, the divergence is avoided and the second threshold appears instead. After the second threshold, the monotonic increase of $\min[2\hbar E_{\boldsymbol{k}}]$ [Fig. 2(c)] indicates the enhancement of the light-induced $e$-$h$ pairing and expands the flattened region of dispersion in Fig. 1(a). It is, then, clear that the plateau of $p_k \approx 0.5$ in Figs. 3(b) and 3(c) is formed by the $e$-$h$ mixing around such flattened dispersions. In the case of $\hbar\kappa = 100$ $\mu$eV, on the other hand, the second threshold is related to the crossover into lasing, explained as follows. Before the second threshold, the system stays in quasiequilibrium (red circles in Fig. 2, $\mu_B - \hbar\omega_{\rm LP} \lesssim 6.0 \times 10^1$ meV), where the relationship between the renormalized band and the pumping baths is well expressed in Fig. 1(c). In this situation, the pumping is blocked inside the gap $\min[2\hbar E_{\boldsymbol{k}}]$. However, by increasing the pumping $\mu_B$, $\mu_B - \mu$ exceed the gap, $\mu_B - \mu \gtrsim \min[2\hbar E_{\boldsymbol{k}}]$, and then, electrons above the gap can be supplied suddenly. Such a feeding mechanism causes a rapid increase of photons, resulting in the second threshold. Here, by ignoring the effects of $\gamma$ and $T$, this situation $\mu_B - \mu \gtrsim \min[2\hbar E_{\boldsymbol{k}}]$ is equivalent to the above-described condition (II) for the lasing phases. Consequently, the second threshold is accompanied by the change into lasing (nonequilibrium). By increasing the pumping further, $\mu$ is fixed around the cavity [Fig. 2(b)], $\min[2\hbar E_{\boldsymbol{k}}]$ is decreased [Fig. 2(c)], and the effective band gap $E_g^* \equiv E_g + \hbar\Sigma^{\rm BGR}_{e,\boldsymbol{k}=0} + \hbar\Sigma^{\rm BGR}_{h,\boldsymbol{k}=0}$ shrinks, of course. The lasing situation is then well captured in Fig. 1(d), where the gap $\min[2\hbar E_{\boldsymbol{k}}]$ is decreased but still opened around the laser frequency. The decrease of the gap for $\mu_B - \mu \gtrsim \min[2\hbar E_{\boldsymbol{k}}]$ implies that the particle flux $\mu_B - \mu$ beyond $\min[2\hbar E_{\boldsymbol{k}}]$ acts toward $e$-$h$ pair breaking but the $e$-$h$ pairs cannot be fully dissociated because $\min[2\hbar E_{\boldsymbol{k}}] \neq 0$. As a result, light-induced $e$-$h$ pairs are still formed around the laser frequency, typically around the energy regions of the kinetic hole burning [Figs. 3(e) and 3(f)]. This is, in turn, somewhat analogous to the $e$-$h$ Cooper pairs formed around the Fermi energy, i.e., weakly correlated $e$-$h$ pairs in momentum space. The difference is that the $e$-$h$ pairs are formed around the laser frequency rather than the Fermi energy.

These results indicate that it would be reasonable to explain the second thresholds reported in current experiments by the crossover into lasing because $\kappa = 100$ $\mu$eV is a reasonable value for them, in agreement with earlier explanations [10,12–15]. Our theory, however, shows that the crossover is not accompanied by the dissociations of bound $e$-$h$ pairs. Instead, the pairing mechanism changes into the light-induced one around the laser frequency. This is in contrast to the commonly accepted ideas but a natural picture of lasing.

We have thus discussed two different types of second thresholds. However, it is difficult to directly distinguish them by the excitation dependence of the number of photons [Fig. 2(a)], in principle. Therefore, we finally study the measurable optical gain spectra $G(\omega)$ [30,31] by assuming an additional perturbative Hamiltonian $\hat{H}'(t) = -F(t)\sum_{\boldsymbol{k}} d_{cv}(\hat{c}^\dagger_{c,\boldsymbol{k}}\hat{c}_{v,\boldsymbol{k}} + \text{H.c.})$. Here, $F(t)$ is the weak light field irradiated from the outside and $d_{cv}$ is the dipole matrix element. Within the linear response [32], $G(\omega)$ is estimated with the ladder approximation [33]. Figures 4(a)–4(f) show the gain spectra corresponding to Figs. 3(a)–3(f), respectively. In the case of $\hbar\kappa = 0.1$ $\mu$eV, two absorption peaks can be found, which result from the two flattened dispersions shown in Fig. 1(a). Therefore, the separation of the peaks corresponds to $\min[4\hbar E_{\boldsymbol{k}}]$, the sum of the gaps in the conduction and valence bands. Here, we note that absorption dominates the spectra because there is no or little population inversion ($n_{e,k} > 0.5$) for the condensed phases in equilibrium [Figs. 3(a)–3(c)]. In the case of $\hbar\kappa = 100$ $\mu$eV, however, gain appears when the system enters into the lasing phase [Figs. 4(e) and 4(f)] although absorption still dominates in the quasiequilibrium case [Fig. 4(d)]. The spectral hole (or gap) with a separation of $\min[4\hbar E_{\boldsymbol{k}}]$ in Fig. 4(f) reflects the gap formed in the

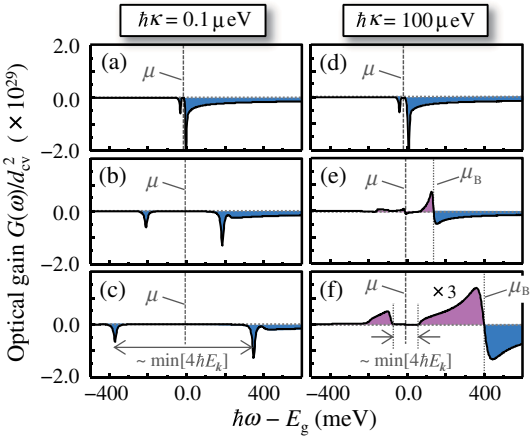


FIG. 4 (color online). Optical gain spectra. Panels (a)–(f) correspond to Figs. 3(a)–3(f), respectively. Positive and negative values represents the gain and absorption, respectively.

renormalized band [Fig. 1(d)]. The existence of the gain after the second threshold is due to the population inversion for lasing [Figs. 3(e) and 3(f)] and, as a result, can be used to distinguish the two types of second thresholds in experiments.

To summarize, we have shown that there are two different types of second thresholds. In both cases, dissociations of bound *e-h* pairs do not occur due to the light-induced pairing, in contrast to earlier expectations. The gain spectra are also studied and the existence of the gain would be useful to distinguish the two different types of second thresholds.

We are grateful to T. Horikiri, Y. Shikano, M. Bamba, T. Yuge, K. Asano, T. Ohashi, H. Akiyama, M. Kuwata-Gonokami, T. Inagaki, P. Huai, H. Ajiki, J. Keeling, and P. B. Littlewood for fruitful discussions. This work is supported by the JSPS through its FIRST Program, and DYCE, KAKENHI No. 20104008.

*yamaguchi@acty.phys.sci.osaka-u.ac.jp

[1] H. Deng, G. Weihs, C. Santori, J. Bloch, and Y. Yamamoto, Science **298**, 199 (2002).
[2] J. Kasprzak *et al.*, Nature (London) **443**, 409 (2006).
[3] R. Balili, V. Hartwell, D. Snoke, L. Pfeiffer, and K. West, Science **316**, 1007 (2007).
[4] S. Utsunomiya *et al.*, Nat. Phys. **4**, 700 (2008).
[5] T. Horikiri, P. Schwendimann, A. Quattropani, S. Höfling, A. Forchel, and Y. Yamamoto, Phys. Rev. B **81**, 033307 (2010).
[6] V. V. Belykh, N. N. Sibeldin, V. D. Kulakovskii, M. M. Glazov, M. A. Semina, C. Schneider, S. Höfling, M. Kamp, and A. Forchel, Phys. Rev. Lett. **110**, 137402 (2013).
[7] W. W. Chow and S. W. Koch, *Semiconductor Laser Fundamentals* (Springer-Verlag, Berlin, 1999).
[8] D. Bajoni, P. Senellart, E. Wertz, I. Sagnes, A. Miard, A. Lemaître, and J. Bloch, Phys. Rev. Lett. **100**, 047401 (2008).
[9] J. Kasprzak, D. D. Solnyshkov, R. Andre, L. S. Dang, and G. Malpuech, Phys. Rev. Lett. **101**, 146404 (2008).
[10] R. Balili, B. Nelsen, D. W. Snoke, L. Pfeiffer, and K. West, Phys. Rev. B **79**, 075319 (2009).
[11] B. Nelsen, R. Balili, D. W. Snoke, L. Pfeiffer, and K. West, J. Appl. Phys. **105**, 122414 (2009).
[12] L. S. Dang, D. Heger, R. Andre, F. Boeuf, and R. Romestain, Phys. Rev. Lett. **81**, 3920 (1998).
[13] J.-S. Tempel *et al.*, Phys. Rev. B **85**, 075318 (2012); J.-S. Tempel, F. Veit, M. Aßmann, L. Erik Kreilkamp, S. Höfling, M. Kamp, A. Forchel, and M. Bayer, New J. Phys. **14**, 083014 (2012).
[14] P. Tsotsis, P. S. Eldridge, T. Gao, S. I. Tsintzos, Z. Hatzopoulos, and P. G. Savvidis, New J. Phys. **14**, 023060 (2012).
[15] E. Kamman, H. Ohadi, M. Maragkou, A. V. Kavokin, and P. G. Lagoudakis, New J. Phys. **14**, 105003 (2012).
[16] H. Deng, H. Haug, and Y. Yamamoto, Rev. Mod. Phys. **82**, 1489 (2010).
[17] M. H. Szymanska, J. Keeling, and P. B. Littlewood, Phys. Rev. Lett. **96**, 230602 (2006); Phys. Rev. B **75**, 195331 (2007).
[18] J. Keeling, M. H. Szymanska, and P. B. Littlewood, in *Keldysh Green's Function's Approach to Coherence in a Nonequilibrium Steady State: Connecting Bose-Einstein Condensation and Lasing*, edited by G. Slavcheva and P. Roussignol, Optical Generation and Control of Quantum Coherence in Semiconductor Nanostructures (Springer-Verlag, Berlin, 2010).
[19] M. Yamaguchi, K. Kamide, T. Ogawa, and Y. Yamamoto, New J. Phys. **14**, 065001 (2012).
[20] K. Kamide and T. Ogawa, Phys. Rev. Lett. **105**, 056401 (2010); Phys. Rev. B **83**, 165319 (2011).
[21] T. Byrnes, T. Horikiri, N. Ishida, and Y. Yamamoto, Phys. Rev. Lett. **105**, 186402 (2010).
[22] In this Letter, the terms *laser* and *lasing* are used only when the condensation is inherently governed by nonequilibrium kinetics. See also the Supplemental Material [23].
[23] See Supplemental Material at http://link.aps.org/supplemental/10.1103/PhysRevLett.111.026404 for details.
[24] A. A. Abrikosov, L. P. Gorkov, and I. E. Dzyaloshinskii, *Methods of Quantum Field Theory in Statistical Physics* (Pergamon, New York, 1975).
[25] M. O. Scully and M. S. Zubairy, *Quantum Optics* (Cambridge University Press, New York, 1977).
[26] S. Schmitt-Rink, D. S. Chemla, and H. Haug, Phys. Rev. B **37**, 941 (1988).
[27] K. Henneberger, F. Herzel, S. Koch, R. Binder, A. Paul, and D. Scott, Phys. Rev. A **45**, 1853 (1992).
[28] T. Horikiri *et al.* (unpublished).
[29] W. W. Chow, H. C. Schneider, S. W. Koch, C.-H. Chang, L. Chrostowski, and C. J. Chang-Hasnain, IEEE J. Quantum Electron. **38**, 402 (2002).
[30] Y. Takahashi, Y. Hayamizu, H. Itoh, M. Yoshita, H. Akiyama, L. N. Pfeiffer, and K. W. West, Appl. Phys. Lett. **86**, 243101 (2005).
[31] M. Yoshita, T. Okada, H. Akiyama, M. Okano, T. Ihara, L. N. Pfeiffer, and K. W. West, Appl. Phys. Lett. **100**, 112101 (2012).
[32] A. Shimizu and T. Yuge, J. Phys. Soc. Jpn. **79**, 013002 (2010).
[33] H. Haug and S. Schmitt-Rink, Prog. Quantum Electron. **9**, 3 (1984).